

## Article

# Research on High-Temperature Rheological Properties of Emulsified Asphalt Mastics and Their Influencing Factors

Qing Wang<sup>1</sup>, Haolei Chang<sup>2</sup>, Decai Wang<sup>3,\*</sup> , Shengneng Hu<sup>3</sup>, Pingrang Wang<sup>4</sup> and Chengshi Zhang<sup>5</sup><sup>1</sup> School of Highway, Henan College of Transportation, Zhengzhou 451460, China; wanglinwq2008@163.com<sup>2</sup> School of Water Conservancy and Environment, Zhengzhou University, Zhengzhou 450001, China; changhaolei@gs.zzu.edu.cn<sup>3</sup> School of Civil Engineering and Communication, North China University of Water Resources and Electric Power, Zhengzhou 450045, China; hushengneng@ncwu.edu.cn<sup>4</sup> School of Civil Engineering and Architecture, Zhengzhou University of Aeronautics, Zhengzhou 450046, China; wpr2002@aliyun.com<sup>5</sup> China Construction Seventh Engineering Division, Co., Ltd., Zhengzhou 450004, China; zhangchengshi@cscec.com

\* Correspondence: wangdecai@ncwu.edu.cn

**Abstract:** The high-temperature rheological properties of emulsified asphalt mastics have a significant impact on the service performance of cold recycled mixtures with asphalt emulsions. In this paper, a dynamic shear rheological (DSR) test and a multiple stress creep recovery (MSCR) test are carried out to analyze the influence of tunneling coal gangue powder (TCGP), portland cement (PC), limestone powder (LP), and four kinds of filler binder ratio (F/B) on the high-temperature rheological properties of emulsified asphalt mastics before and after rolling thin film oven test (RTFOT) ageing. Based on the principle of time–temperature equivalence and a viscoelasticity material model, the main curve of emulsified asphalt mastics under frequency scanning test is established, and the rheological properties of emulsified asphalt mastics in a wide frequency domain are analyzed. Finally, the grey entropy theory is used to quantitatively analyze the correlation between different high temperature performance evaluation indices of emulsified asphalt mastics. The results show that the RTFOT ageing process can significantly enhance the high temperature deformation resistance of emulsified asphalt residue and its mastics. The rutting factor ( $G^*/\sin \delta$ ) of emulsified asphalt mastics increases exponentially with the increase of F/B, while the phase angle is less affected. TCGP mastics and PC mastics have better high temperature performances than those of LP mastics. The most suitable range of F/B is 0.9~1.2 when TCGP is used as the filler, and 1.2~1.5 when PC or LP is used as the filler. Grey entropy correlation analysis shows that there is a good correlation between the two evaluation systems of the DSR test and the MSCR test, and both can evaluate the high-temperature performance of emulsified asphalt mastics.

**Keywords:** cold recycling; emulsified asphalt mastics; high temperature rheological property; multiple stress creep analysis; grey entropy correlation grade



**Citation:** Wang, Q.; Chang, H.; Wang, D.; Hu, S.; Wang, P.; Zhang, C. Research on High-Temperature Rheological Properties of Emulsified Asphalt Mastics and Their Influencing Factors. *Coatings* **2022**, *12*, 635. <https://doi.org/10.3390/coatings12050635>

Academic Editors: Andrea Nobili and Giorgos Skordaris

Received: 2 March 2022

Accepted: 3 May 2022

Published: 5 May 2022

**Publisher's Note:** MDPI stays neutral with regard to jurisdictional claims in published maps and institutional affiliations.



**Copyright:** © 2022 by the authors. Licensee MDPI, Basel, Switzerland. This article is an open access article distributed under the terms and conditions of the Creative Commons Attribution (CC BY) license (<https://creativecommons.org/licenses/by/4.0/>).

## 1. Introduction

In recent years, the demand for technology for emulsified asphalt cold recycling in asphalt pavement maintenance and upgrading is growing, and the scale of applications is increasing. This demand not only provides new technology for old road reconstruction and maintenance, but is also conducive to environmental protection [1–3]. However, the problems of rutting and poor durability caused by insufficient high-temperature deformation resistance of a cold recycled mixture with asphalt emulsions often appear in practical engineering applications, restricting the further application of this technology. Therefore, improving the high-temperature performance of a cold recycled mixture with asphalt emulsions has become an urgent problem to be solved.

Asphalt mastics are micro-dispersion systems in which mineral fillers are dispersed in asphalt. Some studies have shown that asphalt can have good adhesion to other coarse and fine aggregates only when it is adsorbed on the filler surface to form films, and then mixed with the filler to form mastics. The filler type and the F/B affect the performance of asphalt mastics to a great extent, and therefore affect the performance of an asphalt mixture [4]. Previously, researchers in various countries have carried out many studies on modified asphalt mastics systems in hot asphalt mixtures, but fewer studies have considered emulsified asphalt mastics systems composed of residues formed after the demulsification of emulsified asphalt. Brown [5] studied the rheological properties of emulsified asphalt mastics made of asphalt and mineral powder. The results showed that the test data measured by DSR and a bending beam rheometer (BBR) test can both effectively evaluate the rheological properties of emulsified asphalt mastics, and they had good correlation. Chen [6,7] conducted DSR, BBR, and direct tensile tests on the asphalt mastics in Stone Matrix Asphalt (SMA), and found that both the asphalt and the filler types had great influence on the rheological properties and tensile deformation resistance of the mastics. Hu [8] studied the effect of brake pad waste powder (BPWP) as a filler on the viscosity and rheological properties of asphalt mastics through a softening point test, a rotational viscosity test, and a DSR test. The results showed that the addition of BPWP can improve the viscosity and high temperature rheological properties of asphalt mastics, compared with LP. Wang [9] carried out a linear amplitude sweep (LAS) test, a multiple stress creep recovery (MSCR) test, and a low temperature shear stress relaxation (SSR) test on asphalt mastics prepared with different fine solid wastes (FSWs) as fillers, finding that red mud and diatomite as fillers significantly improved the fatigue performance of asphalt mastics when compared with coal fly ash and LP. Yao [10] evaluated the effects of nano clay particles and polymer-modified nano clay particles on the rheological properties and viscosity of asphalt mastics through DSR, BBR, and Brinell rotational viscosity tests. The test results showed that nano clay particles can significantly improve the complex shear modulus and viscosity of asphalt mastics, while the viscosity of asphalt mastics with polymer-modified nano clay particles decreased slightly. Underwood [11] established a mechanical property analysis model to evaluate the damage mechanism of asphalt mastics under repeated loads, finding that the Schapery-type damage method can simulate the fatigue damage process of the mastics material well if the nonlinear viscoelastic response of the material is properly considered. Cheng [12] compared the fatigue behaviors of compacted asphalt mixture samples under actual strain waves and the commonly used haversine wave. The test results showed that the fatigue lives of asphalt mixture samples subjected to the single-axle wave were obviously higher than those subjected to the haversine wave. Alvarez [13] tested the thermodynamic indices of asphalt mastics prepared with three different fillers. The test results showed that the properties and content of mineral fillers significantly affect the water damage resistance and the low-temperature crack resistance of asphalt mastics, as well as the adhesion of asphalt mastics to aggregate. Wang [14] conducted uniaxial creep tests on SMA and an open-graded friction course (OGFC) asphalt mixture at  $-10\text{ }^{\circ}\text{C}$  and  $-15\text{ }^{\circ}\text{C}$ , respectively. The experimental results showed that the test temperature and the material characteristics of the asphalt mastics composition had a great influence on its viscoelasticity. Xu [15] studied the rheological properties of warm-mix recycled asphalt mastics containing a high proportion of recycled pavement material (RAP) and found that the increase of the RAP binder and filler content had a hardening effect on asphalt mastics and significantly reduced their linear viscoelastic strain limit. Sayadi [16] compared the fatigue performance and self-healing ability of asphalt mastics prepared with electric arc furnace dust (EAFD), granite powder, and hydrated lime powder via a time scanning test. The test results showed that the asphalt mastics prepared with EAFD filler had better self-healing and fatigue-damage resistance. Feng [17] studied the high temperature properties of coal gangue powder mastics and limestone powder mastics via a DSR test. The test results showed that the high temperature performance and temperature sensitivity of coal gangue powder asphalt mastics were significantly improved, compared

with limestone powder asphalt mastics. Li [18] found that the replacement of limestone mineral powder with cement can significantly enhance the high-temperature performance of asphalt mastics.

In summary, the current research on asphalt mastics by scholars in various countries mainly focuses on mastics systems in hot mix asphalt mixtures, which involves consideration of the effects of the contents of LP, cement, and some fine solid waste (FSW) as fillers, as well as the effects of modifiers such as fibers and nanoclay particles, on the performance and fatigue failure resistance of asphalt mastics. The construction of performance prediction models of asphalt mastics has also been considered. However, there has been little research on the properties of emulsified asphalt mastics. There are few studies on the high temperature rheological properties and the corresponding evaluation system of emulsified asphalt mastics in a cold regeneration method. Therefore, this paper systematically conducts experimental research on the high temperature rheological properties of asphalt emulsion mortar and the influences of three different filler types and four different powder-to-binder ratios of TCGP, PC, and LP. The mutual substitutability of the three fillers is discussed, especially the utilization value of coal gangue powder as a regenerated filler, which provides a reference for the use of coal gangue powder filler in an emulsified asphalt mixture. Through the grey entropy correlation analysis method, the consistency of two kinds of high temperature performance evaluation indices by the DSR test and the MSCR test in evaluating the high temperature performance of emulsified asphalt mastics was analyzed. This study provides some guidance for accurately evaluating the performance of emulsified asphalt mastics, optimizing the composition design of cold recycled mixtures, and promoting cold recycling engineering applications.

## 2. Materials and Methods

### 2.1. Materials

#### 2.1.1. Matrix Asphalt

A-70 road petroleum asphalt was selected as the matrix asphalt in this study. The basic performance test results and requirements for A-70 asphalt [19] are shown in Table 1.

**Table 1.** Technical indexes of matrix asphalt.

Indexs		Results	Requirements
	Penetration/0.1 mm	66.2	60~80
	Penetration index	0.68	-1.5~1.0
	Ductility/cm	>100	≥100
	Softening point/°C	49.5	≥46
	Mass loss/%	0.2	-0.8~0.8
After RTFOT ageing	Residual penetration ratio/%	71.2	≥61
	Residual ductility/cm	17.7	≥15

#### 2.1.2. Emulsifier

Kzw-8031 cationic slow-cracking cold regeneration emulsifier produced by the Kang Zewei company was selected as the emulsifier in this study. Its basic technical indices are shown in Table 2.

**Table 2.** Technical indices of kzw-8031 emulsifier.

Indices	Results
Appearance	Brown viscous liquid
Solid content	≥70
Amine content/mmol/g	≥5.2
pH (1% aqueous solution)	9~11
Solubility (2% aqueous solution)	Fully soluble in hot water

### 2.1.3. Mineral Filler

In this study, limestone mineral powder, 42.5 # portland cement, and tunneling coal gangue powder (XRD chemical composition analysis results are shown in Table 3) were selected as fillers. These three kinds of fillers were screened by an 0.075 mm sieve, and there was no agglomeration phenomenon. The test results for the apparent density and hydrophilic fillers of the fillers used in this study are shown in Table 4.

**Table 3.** Main chemical composition of tunneling coal gangue powder.

-	SiO <sub>2</sub>	Al <sub>2</sub> O <sub>3</sub>	Fe <sub>2</sub> O <sub>3</sub>	MgO	CaO	Na <sub>2</sub> O	K <sub>2</sub> O
Content/%	38.10	14.53	3.89	0.76	5.91	0.43	0.16

**Table 4.** Apparent density and hydrophilic coefficient of the fillers used in this study.

Indices	Filler Type	Results
Apparent density/g/cm <sup>3</sup>	LP	2.63
	PC	3.05
	TCGP	2.27
Hydrophilic coefficient	LP	0.91
	PC	0.79
	TCGP	0.87

## 2.2. Preparation Processes of Emulsified Asphalt Mastics

### 2.2.1. Preparation Processes of Emulsified Asphalt

In the processes of preparing emulsified asphalt, the content of emulsifier was 3%, the content of asphalt was 62%, and the pH was 2.0–2.5. The relevant processes are shown in Figure 1:

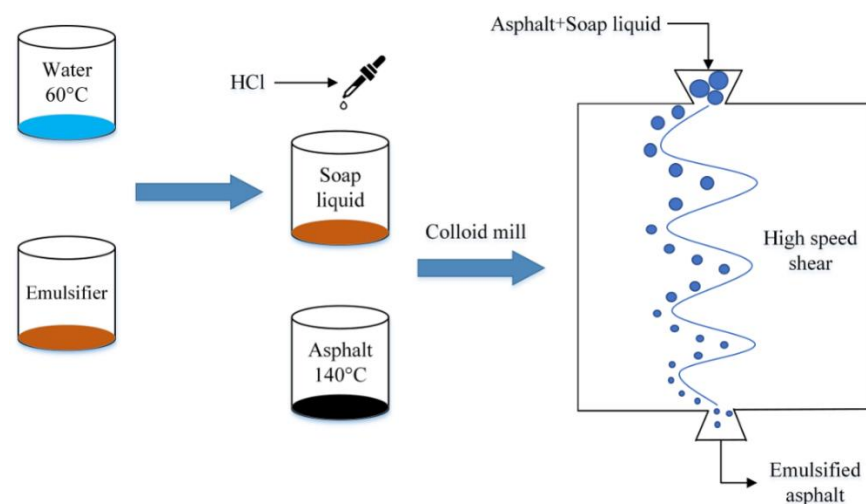


**Figure 1.** Preparation process of emulsified asphalt.

The results of preparing the emulsified asphalt for cold recycling according to the processes in Figure 1 and the testing of its basic technical indices are shown in Table 5.

### 2.2.2. Preparation Processes of Evaporation Residue of Emulsified Asphalt

Preparation of emulsified asphalt residue refers to the direct heating method in JTG E20-2011 [20]. The specific processes were weighing 300 g ± 1 g of emulsified asphalt into a heating dish, placing it in a common heating electric furnace in the laboratory, then heating it slowly and stirring it continuously until the water in the emulsified asphalt evaporated completely, keeping it at 163 ± 3 °C for 1 min at least.

**Table 5.** Performance indices of emulsified asphalt.

Indices		Results	Requirements
Demulsification speed		Slow	Slow or medium
Particle charge		Cation	Cation
Residue on sieve/% (1.18 mm sieve)		0.079	≤0.1
Residue content %		64.8	≥60
Evaporation residue	Penetration/0.1 mm	73.6	50~130
	Ductility/cm	91.5	≥40
Storage stability/%	1 day	0.06	≤1
	5 day	1.01	5

### 2.2.3. Preparation Processes of Emulsified Asphalt Mastics

This study selected four grades of F/B (0.6, 0.9, 1.2, and 1.5) mastics for experimental study. In the processes of preparing the mastics, the most important point was to evenly distribute the filler in each part of the mastics system, which meant that agglomeration and precipitation were not allowed. The preparation processes were as follows.

- (1) Heating the prepared emulsified asphalt residue to 150 °C and keeping it for 1 h to ensure that the residue remained fully flowing and easy to stir.
- (2) Mixing the emulsified asphalt residue with different fillers at 150 °C according to the F/B until there are no bubbles on the surface of the mastics, to ensure the uniform mixing of the emulsified asphalt mastics.

### 2.2.4. RTFOT Short-Term Ageing

The ageing phenomenon of emulsified asphalt mastics during storage, transportation, mixing, and paving was simulated by the short-term ageing test of RTFOT, according to JTG E20-2011 [20].

## 2.3. Test Methods

All groups in this study were set up with three groups of parallel tests, and the test results were taken as the average of the three groups of parallel tests. The STDEV function in ORING software was used to calculate the standard deviation of the three groups of parallel test results, which was used as the error bar in the histogram to reflect the dispersion of test data.

### 2.3.1. Temperature Scanning Test

The temperature sensitivity and viscoelastic properties of emulsified asphalt mastics at different temperatures were evaluated by the temperature scanning function of the DSR test instrument (as shown in Figure 2). The temperature scanning test adopted the strain control mode. The maximum strain was set to 12%, the frequency was 12 rad/s, and the temperature variation range was 58 °C~84 °C for temperature ramp scanning. The test fixture adopted a 25 mm parallel plate, and the spacing was 1 mm.

### 2.3.2. Frequency Scanning Test

The strain of frequency scanning test was set to 0.1%, the test temperature was 20~60 °C, and the gradient was 10 °C. At 20 °C and 30 °C, the test fixture was an 8 mm parallel plate and the gap between the two plates was 2 mm. At 40 °C, 50 °C and 60 °C, the test fixture was a 25 mm parallel plate and the gap between the two plates was 1 mm. The loading frequency range was 0.1–10 Hz.

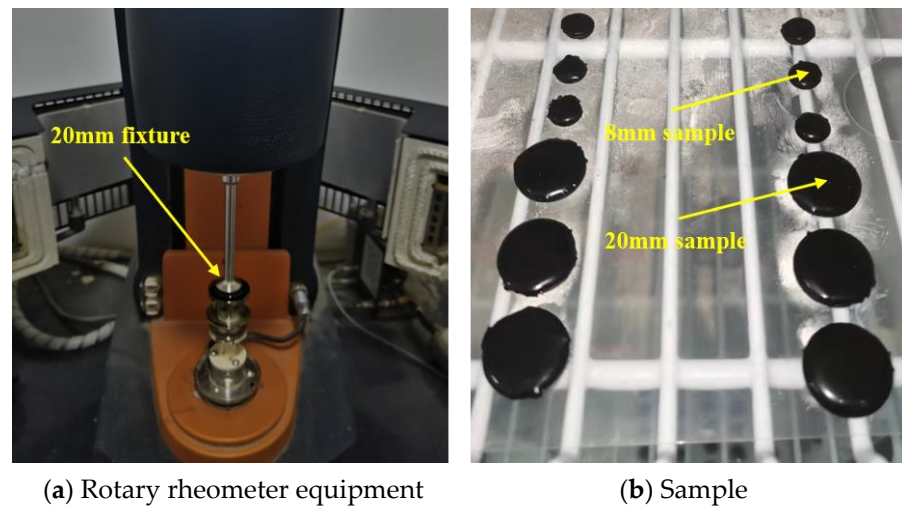


Figure 2. Test instrument and sample of DSR.

### 2.3.3. Main Curve Analysis of Emulsified Asphalt Mastics Based on CAM Model

Based on the time-temperature equivalence principle, the complex shear modulus ( $G^*$ ) curves and the phase angle ( $\delta$ ) curves under different temperatures and load frequencies could be shifted to the same reference temperature to form the main curves of  $G^*$  and  $\delta$ . The horizontal distance between the  $G^*$  and  $\delta$  curves at different temperatures and their corresponding main curves is called the shift factor. The shift factor can be obtained from the Williams–Landel–Ferry (WLF) equation derived from the free volume theory, and its expression is shown in Equation (1).

$$\lg \alpha_T = \frac{-C_1(T - T_0)}{C_2 + (T - T_0)} \quad (1)$$

where  $C_1$  and  $C_2$  represent the fitting parameters related to the temperature sensitivity of the materials;  $T$  ( $^{\circ}\text{C}$ ) represents the testing temperature;  $T_0$  ( $^{\circ}\text{C}$ ) represents the reference temperature; and  $\alpha_T$  represents the shift factor.

The CA model [21–23], the Dickinson and Witt model [24], and other mathematical models are commonly used to describe the rheological properties of asphalt binders. On the one hand, the fitting process requires a large amount of repeated sample data; on the other hand, the fitting process has the disadvantage of poor adaptability to describe the rheological properties of asphalt materials. Therefore, Zeng and Bahia [25] proposed an improved CAM model based on the CA model, which can better describe the rheological properties of matrix asphalt, asphalt mastics, and asphalt mixture. The main curve expressions of  $G^*$  and  $\delta$  in the CAM model are shown in Equations (2)–(4):

$$G^* = G_e^* + \frac{G_g^* - G_e^*}{\left[1 + (f_c/f')^k\right]^{m_e/k}} \quad (2)$$

$$\delta = 90I - (90I - \delta_m) \left\{ 1 + \left[ \frac{\lg(f_d/f')}{R_d} \right]^2 \right\}^{-m_d/2} \quad (3)$$

$$f' = f \times \alpha_T(T) \quad (4)$$

where  $G^*$  (Pa) represents the corresponding complex modulus at frequency  $f'$  (Pa);  $f'$  (Hz) represents the conversion frequency;  $G_g^*$  (Pa) represents the complex modulus of the glassy state when the load frequency approaches infinity;  $G_e^*$  (Pa) represents the platform modulus when the load frequency approaches 0, for asphalt materials  $G_e^* = 0$ ;  $f_c$  (Hz) represents the crossover frequency;  $k$ ,  $m_e$ ,  $R_d$ ,  $m_d$  represent the model parameters;  $\delta$  ( $^{\circ}$ ) represents the

corresponding phase angle at frequency  $f'$ ;  $\delta_m$  ( $^\circ$ ) represents the maximum phase angle;  $f_d$  (Hz) represents the corresponding frequency at the maximum phase angle; and  $I$  represents the indicator factor for asphalt materials (when  $f' > f_d$ ,  $I = 0$ ; when  $f' \leq f_d$ ,  $I = 1$ ).

#### 2.3.4. Multiple Stress Creep Recovery Analysis

The MSCR test was carried out for emulsified asphalt mastics, according to AASHTO MP19-10 [26]. The process involved 10 cycles of 1 s creep cycle and a 9 s recovery cycle at 0.1 kPa and 3.2 kPa stress levels. Test temperatures were 64  $^\circ\text{C}$  and 70  $^\circ\text{C}$ . The evaluation indices included unrecoverable creep compliance ( $J_{nr}$ ) and a creep recovery rate ( $R$ ). The calculation formulae are shown in Equations (5) and (6).

$$J_{nr} = \frac{\gamma_u}{\tau} \quad (5)$$

$$R = \frac{\gamma_p - \gamma_u}{\gamma_p - \gamma_0} \times 100\% \quad (6)$$

where  $\gamma_u$  (%) represents the residual strain;  $\gamma_p$  (%) represents the peak strain;  $\gamma_0$  (%) represents the initial strain; and  $\tau$  (KPa) represents the creep stress.

#### 2.4. Analysis Methods

##### Grey Entropy Correlation Model

The grey correlation analysis method is a new engineering system theory proposed by Professor Deng in 1982. It is mainly used to quantitatively analyze the development trend in the dynamic process, compare the geometric relationship between statistical data in the time series in the system, and quantitatively calculate the correlation degree between the comparison series and the reference series [27,28]. The basic process is as follows: first, the indices to be analyzed are selected as the reference sequence and the comparison sequence, respectively; then, the dimensionless processing of reference sequence and comparison sequence values is carried out; then, the grey correlation coefficient of the reference sequence and the comparison sequence is calculated; and finally, the grey correlation entropy and the grey entropy correlation degree are calculated.

The calculation steps of this method are as follows:

(1) Establish the reference sequence and the comparison sequence.

The comparison sequence and the reference sequence are established according to the principles of system integrity, functionality, accessibility, overlap, and comparability.

Record the reference sequence as:

$$x_0 = (x_{01}, x_{02}, \dots, x_{0n}) \quad (7)$$

where  $x_0$  represents the reference sequence and  $x_{0n}$  represents the test result value of group  $n$  of the reference sequence.

Record the comparison sequence as:

$$x_i = (x_{i1}, x_{i2}, \dots, x_{in}) \quad (8)$$

where  $x_i$  represents the comparison sequence  $i$  and  $x_{in}$  represents the test result value of group  $n$  of the comparison sequence  $i$ .

(2) Carry out the dimensionless process of the reference sequence and the comparison sequence.

In this paper, the mean method was used to carry out the dimensionless process on the data for the reference sequence and the comparison sequence. The calculation Equations are as follows:

$$\bar{x}_{ij} = \frac{1}{n} \sum_{j=1}^n x_{ij} \quad (9)$$

$$x_{ij}' = \frac{x_{ij}}{\bar{x}_{ij}} = (x_i'(1), x_i'(2) \dots x_i'(n)) \quad (10)$$

where  $x_{ij}$  represents the true value of  $j$  sample in index  $i$ ;  $\bar{x}_{ij}$  represents the average value of samples in index  $i$ ; and  $x_{ij}'$  represents the average value of  $j$  sample in index  $i$ .

(3) Calculate the grey correlation coefficient.

First, the absolute value sequence of the difference between the dimensionless values corresponding to  $x_0'$  and  $x_i'$  was calculated

$$\Delta_{ij} = |x_{0j}' - x_{ij}'| \quad (11)$$

Then, the grey correlation coefficient of the comparison sequence and the reference sequence was recorded as:

$$\zeta_{ij}[x_{0j}, x_{ij}] = \left| \frac{\min_{i=1, m, j=1, n} \Delta_{ij} + \rho \max_{i=1, m, j=1, n} \Delta_{ij}}{\Delta_{ij} + \rho \max_{i=1, m, j=1, n} \Delta_i(k)} \right| = \left| \frac{m + \rho M}{\Delta_{ij} + \rho M} \right| \quad (12)$$

where  $\rho = 0.5$  represents the resolution coefficient;  $M$  represents the maximum difference between the two stages; and  $m$  represents the minimum difference between the two stages.

(4) Calculate the grey correlation entropy and the grey entropy correlation degree, as follows:

$$P_{ij} = \frac{\zeta_{ij}[x_{0j}, x_{ij}]}{\sum_{j=1}^n \zeta_{ij}[x_{0j}, x_{ij}]} \quad (13)$$

$$H_i = - \sum_{j=1}^n P_{ij} \ln P_{ij} \quad (14)$$

$$E_i = H_i / H_{\max} \quad (15)$$

where  $P_{ij}$  represents the grey entropy correlation distribution density value;  $H_i$  represents the grey correlation entropy;  $E_i$  represents the grey entropy correlation degree; and  $H_{\max} = \ln n$  represents the maximum value of the grey correlation entropy of the difference information sequence composed of  $n$  elements.

### 3. Results and Discussion

#### 3.1. Temperature Scanning Test

##### 3.1.1. Effect of Temperature on $G^* / \sin \delta$ and $\delta$ of Emulsified Asphalt Mastics

The results of the temperature scanning test are shown in Figures 3–5.

Note: filler binder ratio (F/B); limestone powder (LP); tunneling coal gangue powder (TCGP); portland cement (PC).

The analysis of the temperature scanning test results showed that:

(1) The  $G^* / \sin \delta$  of emulsified asphalt mastics before and after RTFOT ageing decreased gradually, while  $\delta$  increased with the increase in temperature. Because the increase of ambient temperature will aggravate the irregular movement of molecules, this leads to the increase in intermolecular spacing and the volume expansion of the emulsified asphalt residue. As a result, more “holes” are formed inside the residue, which makes the chain segment more prone to displacement under the action of external force, thus reducing the ability of the emulsified asphalt mastics to resist external force [29,30].

(2) After RTFOT ageing,  $G^* / \sin \delta$  of different emulsified asphalt mastics increased significantly, while  $\delta$  decreased by 1–4°. This indicates that the RTFOT ageing process enhances the resistance of emulsified asphalt mastics to high temperature deformation, causing the elastic component of the emulsified asphalt mastics to increase and the viscous component to decrease. This is due to the volatilization of light components in the ageing process, which leads to the increase of asphaltene in the residue and changes the colloidal structure of the residue. Therefore, from the perspective of macro properties, the material becomes hard and brittle [31,32].

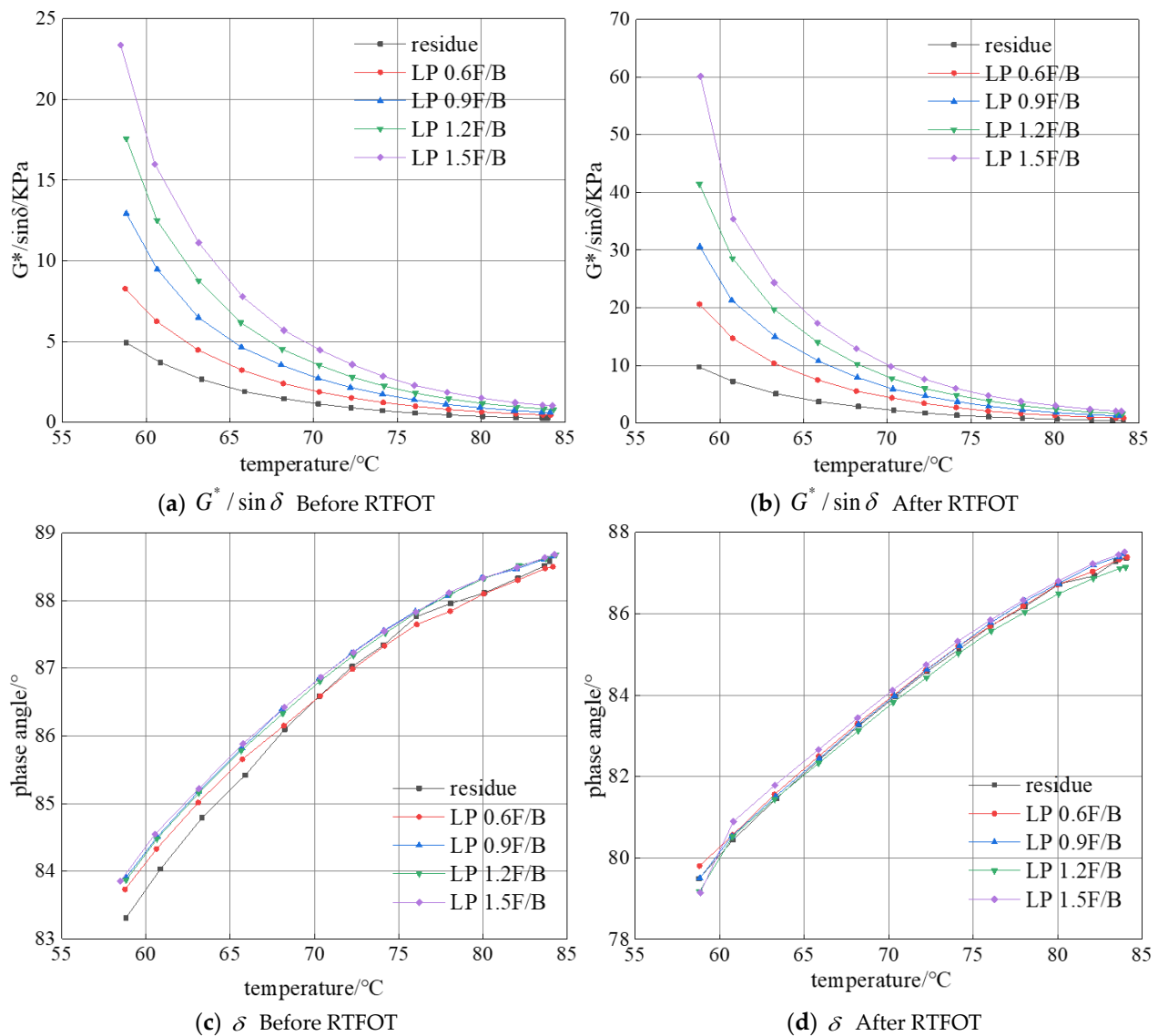


**Figure 3.** Temperature scanning test results of limestone powder asphalt mastics.

(3) After the incorporation of three different fillers, the  $G^*/\sin\delta$  of the emulsified asphalt mastics was significantly increased, and the greater the filler content, the greater the  $G^*/\sin\delta$  of the mastics, indicating that the filler could significantly improve the resistance of the emulsified asphalt mastics to high temperature deformation. However, the addition of fillers had little effect on the  $\delta$  of the mastics. The  $\delta$  represents the viscoelastic composition ratio of the mastics material, indicating that the viscoelastic ratio of the emulsified asphalt mastics prepared by the three fillers selected in this study was independent of the filler content.

### 3.1.2. Influence of Filler Type and Content on $G^*/\sin\delta$ of Emulsified Asphalt Mastics

Figures 6 and 7 show the changes in  $G^*/\sin\delta$  with the increase of the F/B about different mastics.

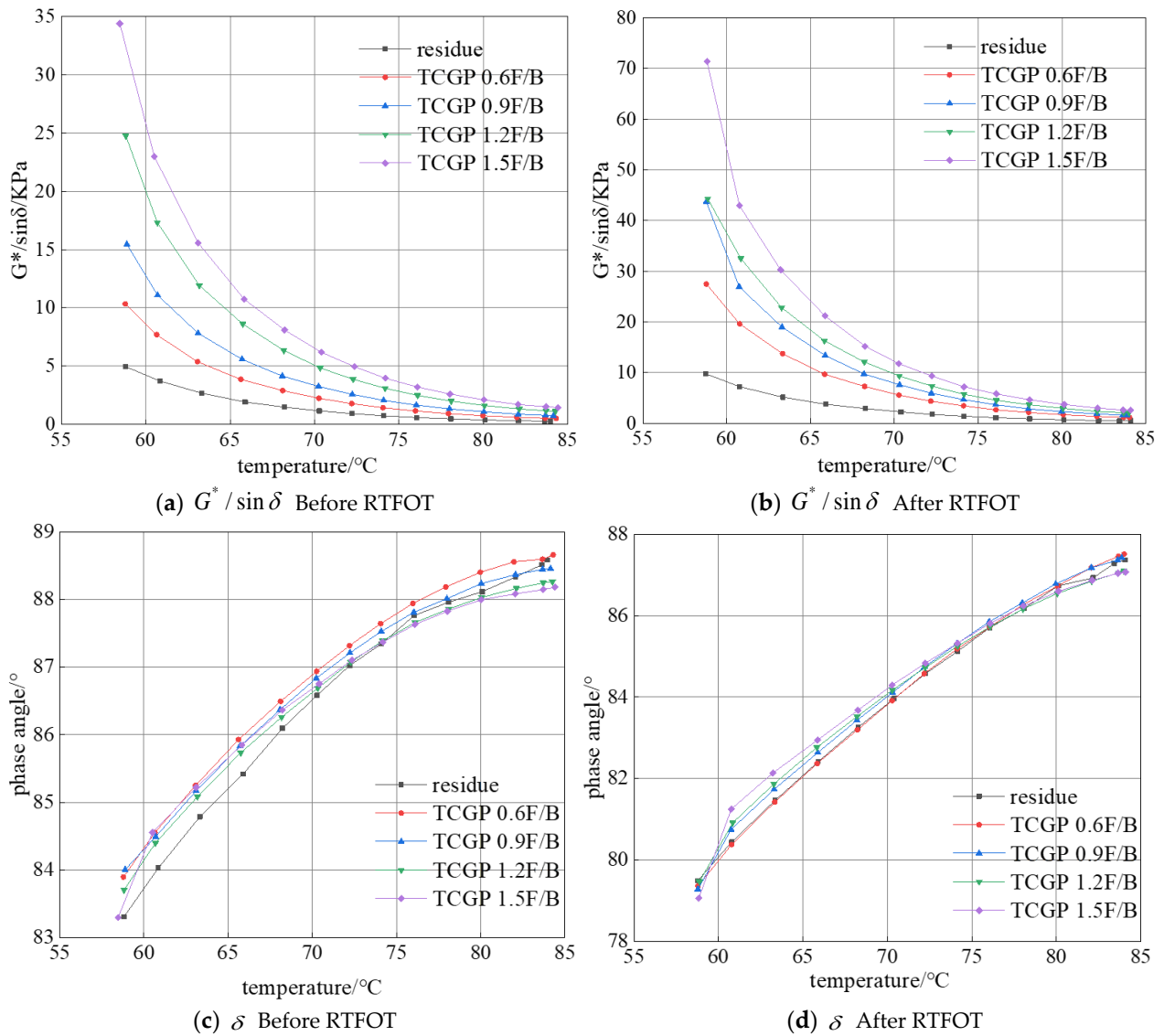


**Figure 4.** Temperature scanning test results of coal gangue powder asphalt mastics.

To further explore the regression relationship between  $G^* / \sin \delta$  and F/B of emulsified asphalt mastics, Equation (16) was selected to fit and analyze the data of  $G^* / \sin \delta$  and F/B [33,34].

$$G^* / \sin \delta = Q \cdot e^{G(F/B)} \tag{16}$$

where F/B represents the mass ratio of the filler to emulsified asphalt residue; Q and G represent the fitting parameters.

The fitting results are shown in Table 6.

It can be seen that there is a strong exponential-function relationship between the  $G^* / \sin \delta$  and the F/B of the emulsified asphalt mastics. The  $R^2$  of each fitting curve was greater than 0.98. This showed that the addition of fillers can significantly enhance the deformation resistance of the emulsified asphalt residue. The high temperature performance of the emulsified asphalt mastics showed strong regularity with the change in F/B and was positively correlated.

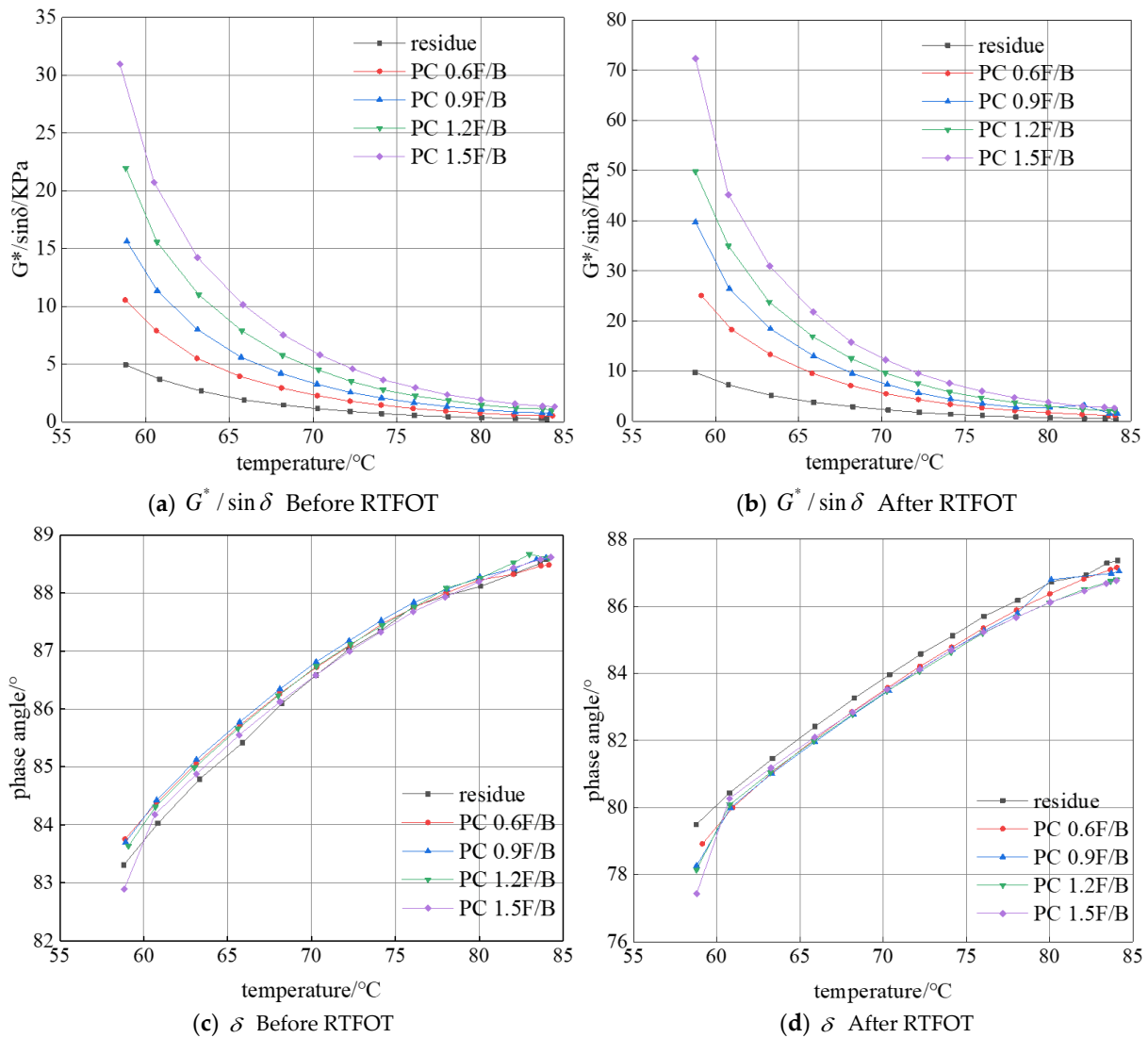


Figure 5. Temperature scanning test results of cement asphalt mastics.

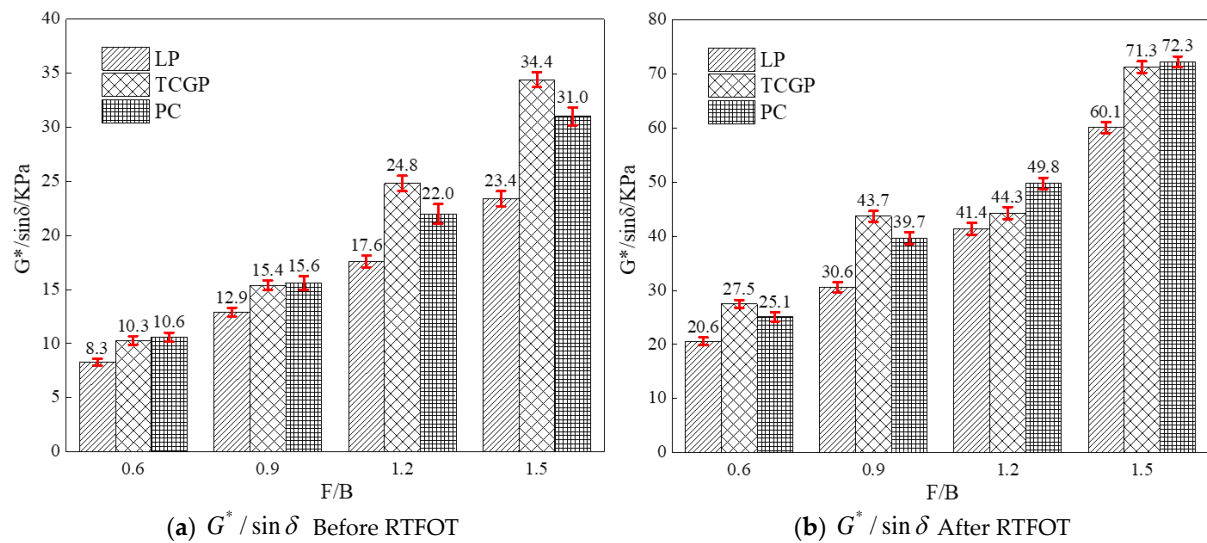


Figure 6. Effect of filler type and F/B on  $G^*/\sin\delta$  of emulsified asphalt mastics (58 °C).

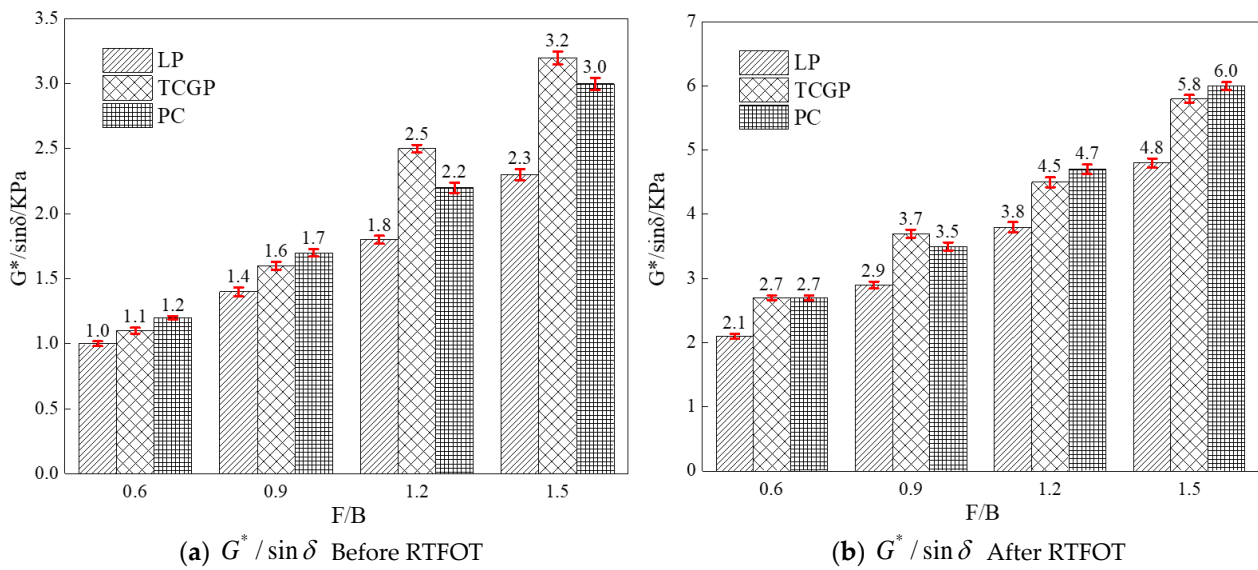


Figure 7. Effect of filler type and F/B on  $G^*/\sin\delta$  of emulsified asphalt mastics (76 °C).

Table 6. Regression Relationship between  $G^*/\sin\delta$  and F/B of emulsified asphalt mastics.

Type of Mastics	Regression Parameter	Before RTFOT		After RTFOT	
		58	76	58	76
LP mastics	Q	4.73	0.61	10.38	1.29
	G	1.07	0.89	1.17	0.88
	R <sup>2</sup>	0.99	1.00	1.00	1.00
TCGP mastics	Q	4.89	0.59	15.67	1.71
	G	1.31	1.14	0.99	0.81
	R <sup>2</sup>	0.99	0.98	0.99	0.99
PC mastics	Q	5.38	0.68	13.62	1.59
	G	1.17	0.99	1.11	0.89
	R <sup>2</sup>	1.00	1.00	1.00	1.00

According to the analysis shown in Figures 6 and 7:

(1) The  $G^*/\sin\delta$  of different emulsified asphalt evaporation residue mastics increased with the increase of the F/B at all temperatures, and the increase was obvious. For example, at 58 °C, the F/B ranged from 0.6 to 1.5, and the  $G^*/\sin\delta$  of TCGP emulsified asphalt mastics before RTFOT ageing increased from 10.3 KPa to 34.4 KPa. It can be seen that the F/B had a great influence on the high temperature deformation resistance of the emulsified asphalt mastics.

(2) Under the same temperature and the same F/B, the  $G^*/\sin\delta$  of the emulsified asphalt residue mastics prepared by different fillers was different. This showed that different fillers have different hardening effects on emulsified asphalt residues. The  $G^*/\sin\delta$  of the TCGP mastics and the cement mastics was significantly greater than that of the LP mastics. Because limestone powder can form a residue mastics system after mixing with residue, which can enhance the anti-dislocation ability of residue molecules, the modulus and strength of the mastics can be greatly improved. After adding TCGP and cement, on the one hand, the modulus enhancement mechanism was similar to that of the LP mastics. On the other hand, the TCGP particles and the cement particles will absorb more light components when coming into contact with emulsified asphalt residues, resulting in an increase in the relative content of gum and asphaltene in the residues, forming more structural asphalt inside the mastics and improving the viscosity of the mastics. Therefore, the increase in modulus and strength will be relatively greater [17,34].

(3) Before RTFOT ageing, when the F/B was 0.6 and 0.9, the  $G^*/\sin\delta$  of the TCGP mastics was slightly less than that of the cement mastics, and the overall difference was small. However, when the F/B was 1.2 and 1.5, the  $G^*/\sin\delta$  of the TCGP mastics was significantly higher than that of the cement mastics. This indicated that the high temperature deformation resistance of the TCGP mastics was more affected by the F/B, compared with the cement mastics. However, the situation changed after RTFOT ageing. The F/B changed from 0.9 to 1.2. The rising trend of  $G^*/\sin\delta$  of TCGP mastics was significantly slower than that of the cement mastics. The  $G^*/\sin\delta$  of TCGP mastics was lower than that of the cement mastics when the F/B was 1.2 and 1.5. The performance of the RTFOT-aged emulsified asphalt mastics was closer to that of emulsified asphalt mastics paved on recycled pavement in practical engineering application. Therefore, it is more appropriate to select the F/B according to the performance of the emulsified asphalt mastics after RTFOT ageing. Further, when the high-temperature performance of the emulsified asphalt mastics was mainly considered, the most suitable range of the F/B was 0.9 to 1.2 when the TCGP was selected as the filler, and the most suitable range of the F/B is 1.2 to 1.5 when limestone powder or cement was selected as the filler.

### 3.2. Frequency Sweep Test

Taking 40 °C as the reference temperature, the shift factors of  $G^*$  and  $\delta$  at each temperature were calculated by the WLF equation, and the translated data were fitted by the CAM model. The principal curves of  $G^*$  and  $\delta$  of the emulsified asphalt evaporation residue mastics were obtained, as shown in Figures 8–10.

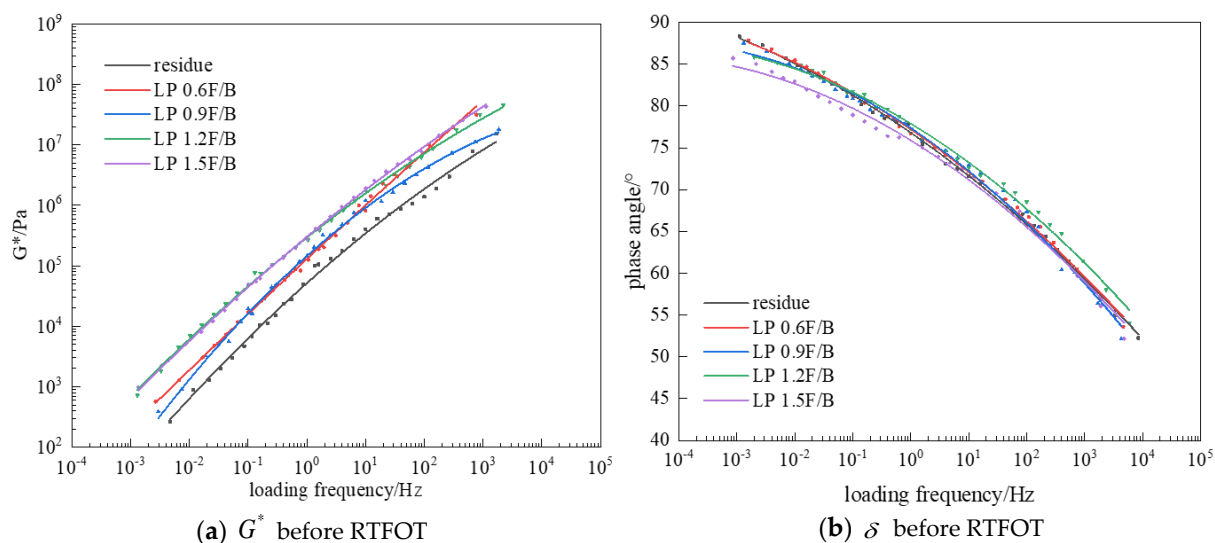


**Figure 8.** Frequency sweep test results of limestone powder emulsified asphalt mastics.

By analyzing and comparing the  $G^*$  and  $\delta$  principal curves of the emulsified asphalt residue mastics, it can be seen that:

(1) The  $G^*$  principal curve and the  $\delta$  principal curve overlap well with the original data, indicating that the  $G^*$  and  $\delta$  of emulsified asphalt mastics are suitable for the CAM model in a wide frequency range.

(2) The  $G^*$  of different kinds of emulsified asphalt mastics increases with the increase of load frequency. Comparing the  $G^*$  fitting curve of the residue and the emulsified asphalt mastics, it can be found that the  $G^*$  of the emulsified asphalt mastics improves in varying degrees compared with the residue in both the high frequency and low frequency ranges.

(3) The  $\delta$  of different emulsified asphalt mastics decreases with the increase in load frequency. In the low frequency range, the  $\delta$  of different F/B emulsified asphalt mastics are obviously different, showing a trend that the larger the F/B, the smaller the  $\delta$ . In the medium and high frequency range, there is little difference in the  $\delta$  of different F/B

emulsified asphalt mastics. This shows that filler content has great influence on the viscosity and elastic ratio of emulsified asphalt mastics under low frequency load.

(4) The  $G^*$  of different kinds of emulsified asphalt mastics increases with the increase in the F/B. The  $G^*$  of the TCGP mastics and the cement mastics is significantly greater than that of the LP mastics, which is consistent with the temperature scanning test results above.

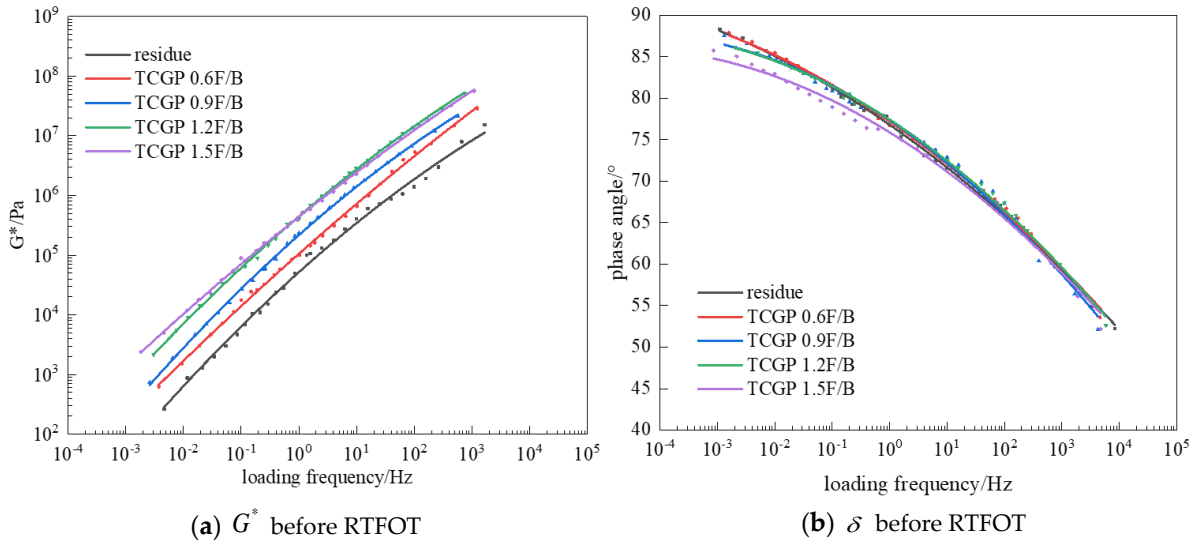


Figure 9. Frequency sweep test results of coal gangue powder emulsified asphalt mastics.

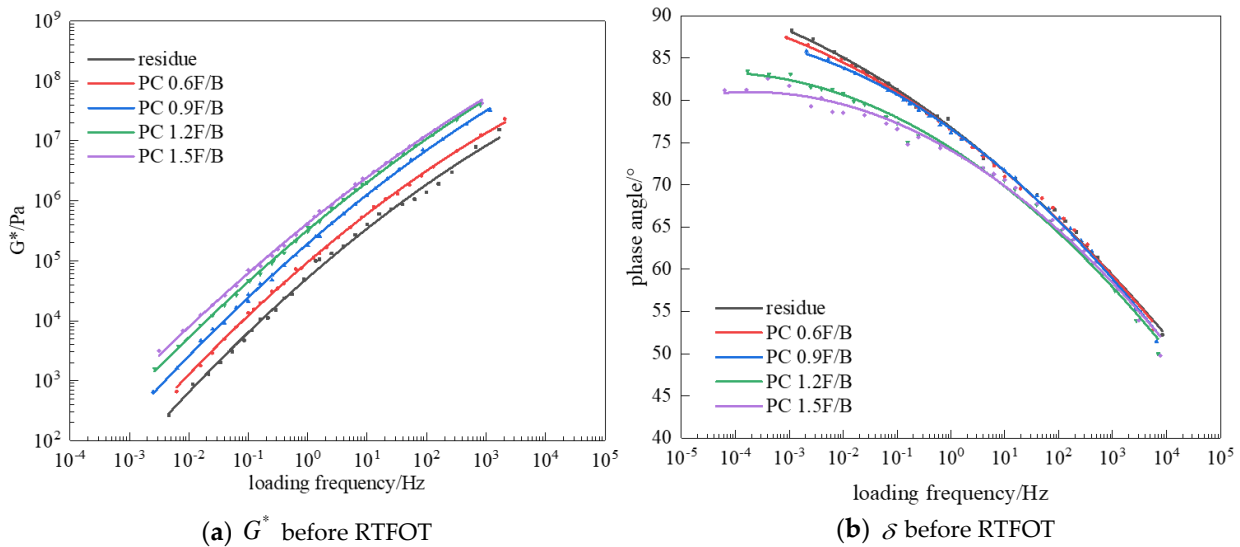


Figure 10. Frequency sweep test results of cement emulsified asphalt mastics.

### 3.3. Multiple Stress Creep Recovery Test

#### 3.3.1. Irrecoverable Creep Compliance

We calculated the irrecoverable creep compliance ( $J_{nr}$ ) of the emulsified asphalt mastics for cold regeneration, according to Equation (5). The test results are shown in Figures 11 and 12.

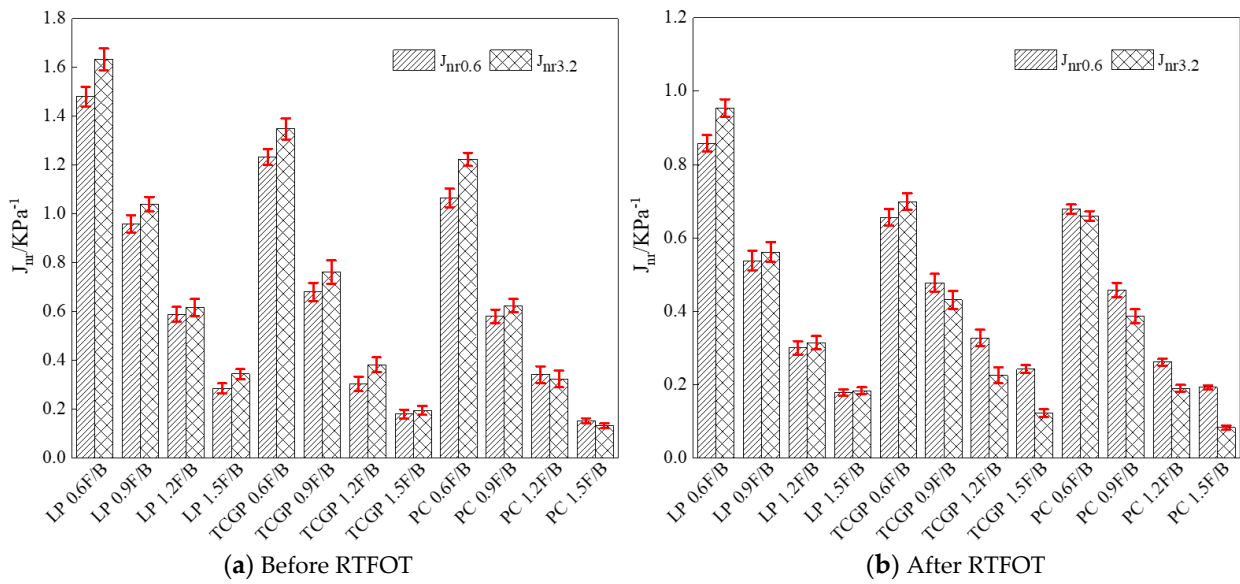


Figure 11. Test results of  $J_{nr}$  of different emulsified asphalt mastics (64 °C).

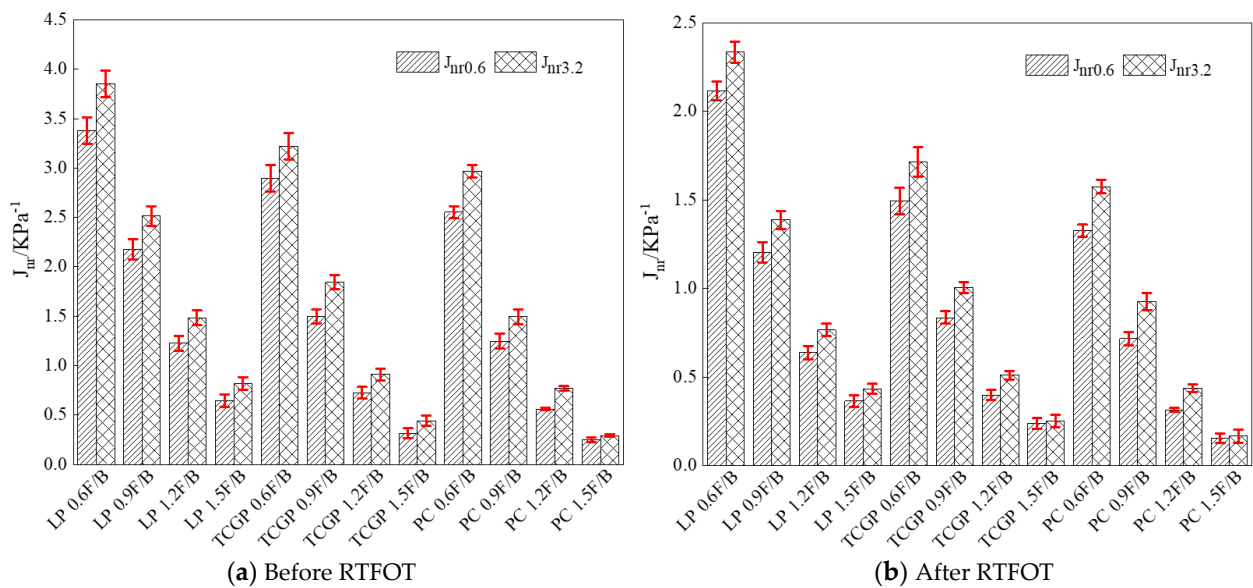


Figure 12. Test results of  $J_{nr}$  of different emulsified asphalt mastics (70 °C).

It can be seen from Figures 11 and 12 that:

(1) Under the same temperature and stress conditions, the  $J_{nr}$  of different emulsified asphalt mastics after RTFOT ageing is significantly reduced, indicating that the RTFOT ageing process can significantly improve the deformation resistance of emulsified asphalt mastics.

(2) The larger the F/B of the emulsified asphalt mastics, the smaller the  $J_{nr}$ , and the stronger its deformation resistance. The higher the temperature, the greater the  $J_{nr}$  of the emulsified asphalt mastics and the worse the deformation resistance.

(3) Before RTFOT ageing, under the same F/B, the order of  $J_{nr}$  of the emulsified asphalt mastics prepared with different fillers was as follows: LP mastics > TCGP mastics > cement mastics. The difference was obvious. After RTFOT ageing, the  $J_{nr}$  of the TCGP mastics and the cement mastics was still significantly lower than that of the LP mastics, indicating that the deformation resistance and the high temperature performance of the TCGP mastics and the cement mastics are significantly better than those of the LP mastics. When the F/B was 0.6 and 0.9, the  $J_{nr}$  of the TCGP mastics was only slightly higher than that of the cement mastics, which indicated that an appropriate content of tunneling coal

gangue powder as filler can effectively improve the deformation resistance of the emulsified asphalt mastics. This also shows the consistency between  $J_{nr}$  and  $G^* / \sin \delta$  in evaluating the high-temperature performance of mastics.

### 3.3.2. Creep Recovery Rate

According to Equation (6), the creep recovery rate (R) of different emulsified asphalt evaporation residue mastics for cold recycling were calculated, as shown in Figures 13 and 14:

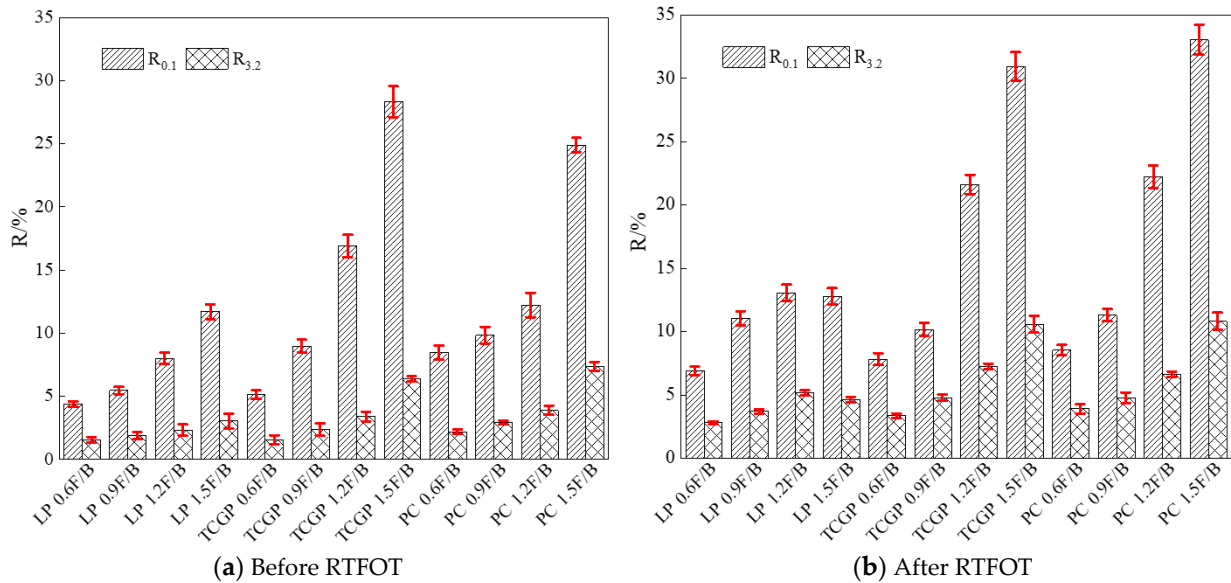


Figure 13. Test results of R of different emulsified asphalt mastics (64 °C).

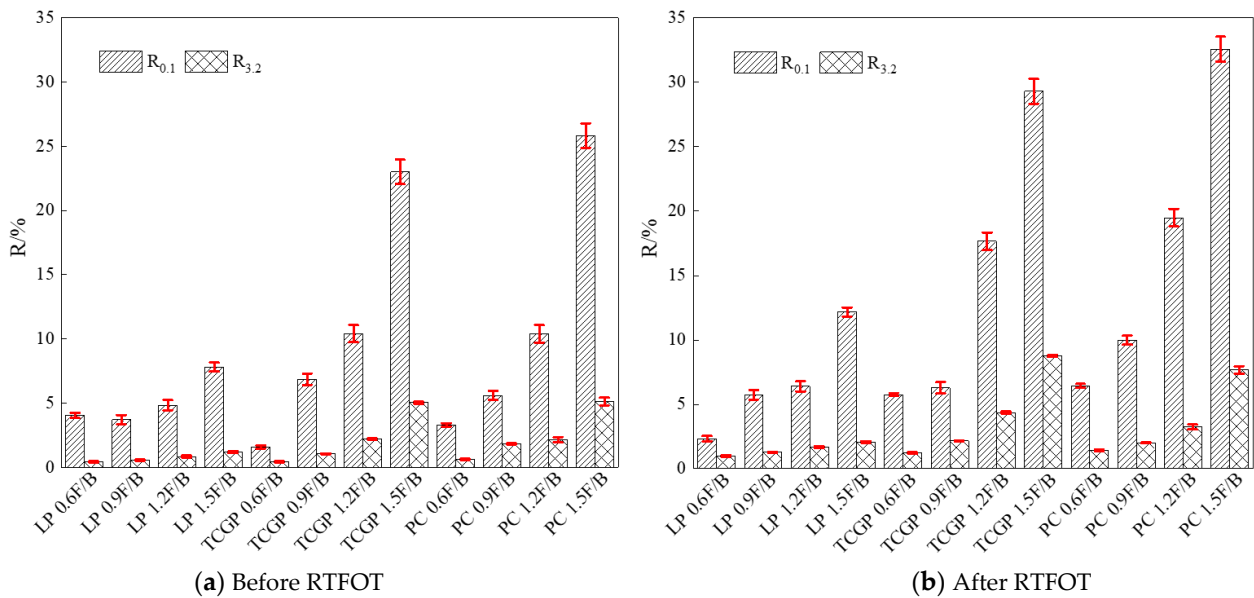


Figure 14. Test results of R of different emulsified asphalt mastics (70 °C).

It can be seen from Figures 13 and 14 that:

(1) Except for 1.2 and 1.5 F/B LP mastics after RTFOT ageing, other groups of emulsified asphalt mastics showed the trend of larger F/Bs and larger Rs when the filler type was the same, indicating that the addition of a filler can significantly improve the deformation recovery ability of the emulsified asphalt mastics.

(2) After RTFOT ageing, the R of emulsified asphalt mastics with different components increased to varying degrees, indicating that the ageing process of RTFOT will improve the deformation recovery ability of the emulsified asphalt mastics.

(3) Under the same stress level, the R of the emulsified asphalt mastics decreased with the increase in temperature, indicating that the increase in temperature increases the viscosity component of the emulsified asphalt mastics, reduces the elastic component, and reduces the high temperature deformation resistance and deformation recovery ability. The R of the emulsified asphalt mastics under the stress level of 3.2 kpa was significantly lower than the stress level of 0.1 kpa, indicating that the greater the stress, the more likely the emulsified asphalt mastics are to produce irreversible deformation.

(4) The type of filler greatly affected the R of the emulsified asphalt mastics, especially at the stress level of 0.1 kpa. Under the same F/B, the R of the TCGP mastics and the cement mastics was significantly higher than that of the LP mastics, indicating that the high-temperature deformation resistance and deformation recovery performance of the TCGP mastics and the cement mastics are significantly higher than those of the LP mastics.

#### 4. Grey Entropy Correlation Analysis

Based on the grey entropy theory, this study carried out a grey correlation analysis on the test results of three high-temperature performance evaluation indices of emulsified asphalt mastics before and after RTFOT ageing:  $G^* / \sin \delta$  at 64 °C, and  $J_{nr}$  and R at the 3.2 kpa stress level. We explored the rationality of different performance evaluation indices of emulsified asphalt mastics and the correlation between various indices. The calculation steps were as follows:

(1) Establish reference sequence and comparison sequence.

Set  $G^* / \sin \delta$  as the reference sequence, and  $J_{nr}$  and R as the comparison sequence. The obtained data are shown in Table 7:

**Table 7.** Original data of rheological properties of emulsified asphalt mastics.

Type of Mastics	Reference Sequence	Comparison Sequence	
	$G^* / \sin \delta$	$J_{nr3.2}$	$R_{3.2}$
Residue	2661.2	4.87820	0.00451
LP 0.6F/B	4481.9	1.63257	0.01576
LP 0.9F/B	6488.2	1.04025	0.01886
LP 1.2F/B	8774.5	0.61729	0.02336
LP 1.5F/B	11,126.3	0.34445	0.03044
TCGP 0.6F/B	5370.7	1.34846	0.01557
TCGP 0.9F/B	7810.3	0.76206	0.02382
TCGP 1.2F/B	11,916.5	0.38242	0.03423
TCGP 1.5F/B	15,577.6	0.19586	0.06386
PC 0.6F/B	5503.8	1.22398	0.02203
PC 0.9F/B	7989.2	0.62527	0.02945
PC 1.2F/B	11,006.6	0.32419	0.03904
PC 1.5F/B	14,218.6	0.13235	0.0738
Residue (RTFOT)	5128.6	2.24137	0.00644
LP 0.6F/B(RTFOT)	10,374.7	0.95427	0.02809
LP 0.9F/B(RTFOT)	15,011.4	0.56175	0.03699
LP 1.2F/B(RTFOT)	19,722.1	0.31420	0.05164
LP 1.5F/B(RTFOT)	24,371.1	0.18385	0.04652
TCGP 0.6F/B(RTFOT)	13,726.0	0.69893	0.03363
TCGP 0.9F/B(RTFOT)	18,967.1	0.43091	0.04806
TCGP 1.2F/B(RTFOT)	22,822.8	0.22564	0.0726
TCGP 1.5F/B(RTFOT)	30,267.0	0.12185	0.10594
PC 0.6F/B(RTFOT)	13,309.4	0.65983	0.03911
PC 0.9F/B(RTFOT)	18,414.6	0.38682	0.04793
PC 1.2F/B(RTFOT)	23,750.6	0.19014	0.06654
PC 1.5F/B(RTFOT)	30,946.9	0.08332	0.10843

(2) Dimensionless processing of reference sequence and comparison sequence.

According to the Equation (9) and Equation (10), the original data in Table 7 are dimensionless.

(3) Calculate the grey correlation coefficient.

The grey correlation coefficient between the comparison sequence and the reference sequence can be obtained by substituting the dimensionless rheological property index data in Table 8 into Equations (11) and (12) for calculation.

**Table 8.** The rheological property index of emulsified asphalt mastics after dimensionless treatment.

Type of mastics	Reference Sequence	Comparison Sequence	
	$G^*/\sin\delta$	$J_{nr3.2}$	$R_{3.2}$
Residue	0.19	6.17	0.11
LP 0.6F/B	0.33	2.06	0.38
LP 0.9F/B	0.47	1.32	0.45
LP 1.2F/B	0.64	0.78	0.56
LP 1.5F/B	0.81	0.44	0.73
TCGP 0.6F/B	0.39	1.71	0.37
TCGP 0.9F/B	0.57	0.96	0.57
TCGP 1.2F/B	0.87	0.48	0.82
TCGP 1.5F/B	1.13	0.25	1.53
PC 0.6F/B	0.40	1.55	0.53
PC 0.9F/B	0.58	0.79	0.70
PC 1.2F/B	0.80	0.41	0.93
PC 1.5F/B	1.03	0.17	1.77
Residue (RTFOT)	0.37	2.83	0.15
LP 0.6F/B(RTFOT)	0.75	1.21	0.67
LP 0.9F/B(RTFOT)	1.08	0.71	0.89
LP 1.2F/B(RTFOT)	1.42	0.40	1.24
LP 1.5F/B(RTFOT)	1.76	0.23	1.11
TCGP 0.6F/B(RTFOT)	0.99	0.88	0.80
TCGP 0.9F/B(RTFOT)	1.37	0.54	1.15
TCGP 1.2F/B(RTFOT)	1.65	0.29	1.74
TCGP 1.5F/B(RTFOT)	2.19	0.15	2.53
PC 0.6F/B(RTFOT)	0.96	0.83	0.94
PC 0.9F/B(RTFOT)	1.33	0.49	1.15
PC 1.2F/B(RTFOT)	1.71	0.24	1.59
PC 1.5F/B(RTFOT)	2.23	0.11	2.59

(4) Calculate the grey correlation entropy and the grey entropy correlation degree.

Substituting the calculation results of the grey correlation coefficient between each comparison sequence and reference sequence in (3) into Equations (13) to (15), the calculation results of the grey entropy correlation degree between other rheological performance indices of emulsified asphalt mastics and the  $G^*/\sin\delta$  can be obtained, as shown in Table 9.

**Table 9.** Calculation results of grey entropy correlation degree.

Evaluating Indicator	$J_{nr3.2}$	$R_{3.2}$
Grey entropy correlation degree	0.9937	0.9996

It can be seen from Table 9 that the correlation degree between the  $G^*/\sin\delta$  and other high temperature performance evaluation indices of emulsified asphalt mastics is greater than 0.99. In other words, there is a good correlation between the temperature scanning test evaluation index  $G^*/\sin\delta$  and the MSCR test evaluation system of emulsified asphalt mastics. Both of the test methods can accurately evaluate the high-temperature rheological properties of emulsified asphalt mastics.

## 5. Conclusions

In this study, the DSR and MSCR tests were used to systematically study the influence of the TCGP, PC, LP, F/B, and RTFOT ageing processes on the high-temperature rheological properties of emulsified asphalt mastics for cold recycling, and the optimum content of different mineral fillers was obtained, providing some references for the material composition design of the emulsified asphalt cold recycled mixture. The main conclusions of this study are summarized as follows:

(1) After RTFOT ageing, the high-temperature performance of emulsified asphalt mastics was improved and the viscoelasticity ratio was reduced. The  $G^*/\sin \delta$  of emulsified asphalt mastics increased exponentially with the increase of the F/B while the phase angle was less affected.

(2) Compared with the evaporation residue of emulsified asphalt, the  $G^*/\sin \delta$  and the R of emulsified asphalt mastics increased, the  $J_{nr}$  decreased with the increase of the filler content, and its high-temperature performance was significantly improved, while the addition of filler had little effect on the viscoelastic ratio of the mastics.

(3) At the same F/B and temperature, compared with LP mastics, the  $G^*$ ,  $G^*/\sin \delta$  and the R of the TCGP and the cement mastics were higher, the  $J_{nr}$  was lower, and their high-temperature rheological properties were significantly better than the LP mastics. Considering the high temperature performance of emulsified asphalt mastics, when the TCGP was selected as the filler, the most appropriate range of the F/B is 0.9~1.2, and when the LP or cement was the filler, the most appropriate range of F/B was 1.2~1.5.

(4) The  $G^*$  and  $\delta$  of emulsified asphalt mastics were suitable for a CAM model in a wide frequency range. In the low frequency range, the larger the F/B of emulsified asphalt mastics, the smaller the  $\delta$ , while in the medium and high frequency range, the  $\delta$  of emulsified asphalt mastics with different F/Bs was almost the same.

(5) It was proved that the evaluation indicator of the DSR test of the emulsified asphalt mastics had a good correlation with the evaluation indicator of the MSCR test, based on the grey entropy theory. Both test methods can accurately evaluate the high temperature performance of emulsified asphalt mastics.

The research on the influence of filler type and content on the low-temperature performance, fatigue performance, and microstructure of emulsified asphalt mastics was not involved in this paper. In the next step, it will be necessary to carry out research on the low-temperature performance and fatigue performance of emulsified asphalt mastics, and to study the microscopic mechanisms of emulsified asphalt mastics.

**Author Contributions:** Q.W. and D.W. conceived and designed the research; Q.W. and H.C. drafted the manuscript and prepared figures; H.C. and D.W. reviewed and edited the manuscript; S.H., P.W. and C.Z. discussed the results. All authors have read and agreed to the published version of the manuscript.

**Funding:** This study was supported by the Key Research and Development Project of Henan Province (Program No. 222102320407), North China University of Water Resources and Electric Power High-level Talent Research Start-up Project (202009005), and by the Key Research Project of Institutions of Higher Education in Henan Province (Program No. 20A580003).

**Institutional Review Board Statement:** Not applicable.

**Informed Consent Statement:** Not applicable.

**Data Availability Statement:** Not applicable.

**Conflicts of Interest:** The authors declare no conflict of interest.

## References

1. Ayar, P. Effects of additives on the mechanical performance in recycled mixtures with bitumen emulsion: An overview. *Constr. Build. Mater.* **2018**, *178*, 551–561. [[CrossRef](#)]
2. Tao, J.; Bin, S.; Lijun, S. Technology of Emulsified Asphalt Cold Recycling Upper Base Used in Expressway Asphalt Pavement Heavy Maintenance. In *International Conference on Measuring Technology & Mechatronics Automation*; IEEE: New York, NY, USA, 2011.

3. Carvajal, M.E. *Evaluation of Cracking Behavior of Cold In-Place Recycling Asphalt Mixtures*; University of Nevada: Reno, Nevada, 2018.
4. Zou, G.; Zhang, X.; Han, C. Utilization of DSR for evaluation of pavement performance. *J. Harbin Univ. Civ. Eng. Archit.* **2001**, *34*, 112–115.
5. Brown, E.R.; Haddock, J.E.; Campbell, C. Investigation of Stone Matrix Asphalt Mastics. *Transp. Res. Rec.* **1996**, *1530*, 95–102. [[CrossRef](#)]
6. Chen, J.S.; Peng, C.H. Analyses of tensile failure properties of asphalt-mineral filler mastic. *J. Mater. Civ. Eng.* **1998**, *10*, 256–262. [[CrossRef](#)]
7. Chen, J.S. Rheological properties of asphalt-mineral filler mastics. *Proc. Jpn. Soc. Civ. Eng.* **1997**, *571*, 269–277. [[CrossRef](#)]
8. Hu, X.; Wang, N.; Pan, P.; Bai, T. Performance evaluation of asphalt mixture using brake pad waste as mineral filler. *Constr. Build. Mater.* **2017**, *138*, 410–417. [[CrossRef](#)]
9. Wang, H.; Li, H.; Zhang, H.; Zhang, X.; Guo, B.; Yu, B.; Liu, L.; Tian, Y. Experimental study on the aging behavior of modified asphalt with different types of fine solid wastes under different aging conditions. *Constr. Build. Mater.* **2021**, *291*, 123308. [[CrossRef](#)]
10. Yao, H.; You, Z.; Li, L.; Shi, X.; Goh, S.W.; Mills-Beale, J.; Wingard, D. Performance of asphalt binder blended with non-modified and polymer-modified nanoclay. *Constr. Build. Mater.* **2012**, *35*, 159–170. [[CrossRef](#)]
11. Underwood, B.S. A continuum damage model for asphalt cement and asphalt mastic fatigue. *Int. J. Fatigue* **2016**, *82*, 387–401. [[CrossRef](#)]
12. Cheng, H.L.; Sun, L.J.; Wang, Y.H.; Chen, X. Effects of actual loading waveforms on the fatigue behaviours of asphalt mixtures. *Int. J. Fatigue* **2021**, *151*, 106386. [[CrossRef](#)]
13. Alvarez, A.E.; Ovallera, E.; Caro, S. Assessment of the effect of mineral filler on asphalt—aggregate interfaces based on thermodynamic properties. *Constr. Build. Mater.* **2012**, *28*, 599–606. [[CrossRef](#)]
14. Wang, H.; Hao, P.; You, Z. Characterization of the viscoelastic property of asphalt mastic. *Pavement Mater.* **2011**, *212*, 115–122.
15. Xu, H.; Chen, J.; Sun, Y.; Zhu, X.; Wang, W.; Liu, J. Rheological and physico-chemical properties of warm-mix recycled asphalt mastic containing high percentage of RAP binder. *J. Clean. Prod.* **2020**, *289*, 125134. [[CrossRef](#)]
16. Sayadi, M.; Hesami, S. Performance evaluation of using electric arc furnace dust in asphalt binder. *J. Clean. Prod.* **2016**, *143*, 1260–1267. [[CrossRef](#)]
17. Feng, X.J.; Zhao, M.L.; Chen, W.; Xie, M. Research of road performances and microcosmic mechanisms of coal waste powder asphalt mortar. *J. Build. Mater.* **2019**, *22*, 113–119.
18. Li, Q.R.; Xu, X.Q.; Ji, X.P. Effect of Cement and Slaked Lime on Rheological Properties of Asphalt Mortar. *J. Wuhan Univ. Technol.* **2021**, *45*, 99–104.
19. *JTG F40-2019*; Technical Specifications for Construction of Highway Asphalt Pavements. Ministry of Transport of the People’s Republic of China: Beijing, China, 2019.
20. *JTG E20-2011*; Standard Test Methods of Bitumen and Bituminous Mixtures for Highway Engineering. Ministry of Transport of the People’s Republic of China: Beijing, China, 2011.
21. Sudarsanan, N.; Fonte, B.R.; Kim, Y.R. Application of time-temperature superposition principle to pull-off tensile strength of asphalt tack coats. *Constr. Build. Mater.* **2020**, *262*, 120798. [[CrossRef](#)]
22. Graziani, A.; Canestrari, F.; Cardone, F.; Ferrotti, G. Time-temperature superposition principle for interlayer shear strength of bituminous pavements. *Road Mater. Pavement Des.* **2017**, *18*, 12–25. [[CrossRef](#)]
23. Dickinson, E.J.; Witt, H.P. The dynamic shear modulus of paving asphalts as a function of frequency. *Trans. Soc. Rheol.* **1974**, *18*, 591–606. [[CrossRef](#)]
24. Zho, J.; Wang, D.; Bai, Q. Research on Master Curve of Dynamic Modulus of Asphalt Mixture. *Highw. Eng.* **2009**, *34*, 60–62.
25. Zeng, M.; Bahia, H.U.; Zhai, H.; Turner, P. Rheological modeling of modified asphalt binders and mixtures (with discussion). *J. Assoc. Asph. Paving Technol.* **2001**, *70*, 8–35.
26. American Association of State Highway and Transportation Officials (AASHTO). *Standard Specification for Performance-Graded Asphalt Binder Using Multiple Stress Creep Recovery (MSCR) Test*; AASHTO MP19-10; AASHTO: Washington DC, USA, 2010.
27. Tian, Z. *Research of Transport Structure Based on Information Entropy and Grey Relevance*; Inner Mongolia University: Hohhot, China, 2013.
28. Zhang, Q.; Deng, J. Grey relation entropy method of grey relation analysis. *Syst. Eng. Theory Pract.* **1996**, *36*, 8–12.
29. Zhang, H.P.; Liu, Y.; Deng, Y. Temperature gradient modeling of a steel box-girder suspension bridge using Copulas probabilistic method and field monitoring. *Adv. Struct. Eng.* **2020**, *24*, 947–961. [[CrossRef](#)]
30. Zhu, C.; Xu, G.; Zhang, H.; Xiao, F.; Amirkhanian, S.; Wu, C. Influence of different anti-stripping agents on the rheological properties of asphalt binder at high temperature—ScienceDirect. *Constr. Build. Mater.* **2018**, *164*, 317–325. [[CrossRef](#)]
31. Wang, H.; Ma, Y.; Sun, C. Influence of aging on conventional and rheological properties of asphalt. *Sci. Technol. Innov.* **2021**, *32*, 143–144.
32. Cui, Y.; Guo, L.; Chen, D. Composite aging mechanism of SBS modified asphalt. *J. Build. Mater.* **2020**, *23*, 1183–1191.
33. Liu, J. *Research on Rheological Characteristic of Polyphosphoric Acid Modified Asphalt Mortar*; Hunan University: Changsha, China, 2017.
34. Ye, Q. *Research on the Rheological Characteristics of Fiber Modified Asphalt Binder and Mixture*; Wuhan University of Technology: Wuhan, China, 2007.